

HERMES: A Unified Self-Driving World Model for Simultaneous 3D Scene Understanding and Generation

Xin Zhou^{1*}, Dingkang Liang^{1*†}, Sifan Tu¹, Xiwu Chen³, Yikang Ding^{2†},
Dingyuan Zhang¹, Feiyang Tan³, Hengshuang Zhao⁴, Xiang Bai^{1✉}

¹ Huazhong University of Science and Technology, ² MEGVII Technology,
³ Mach Drive, ⁴ The University of Hong Kong
{xzhou03, dkliang}@hust.edu.cn

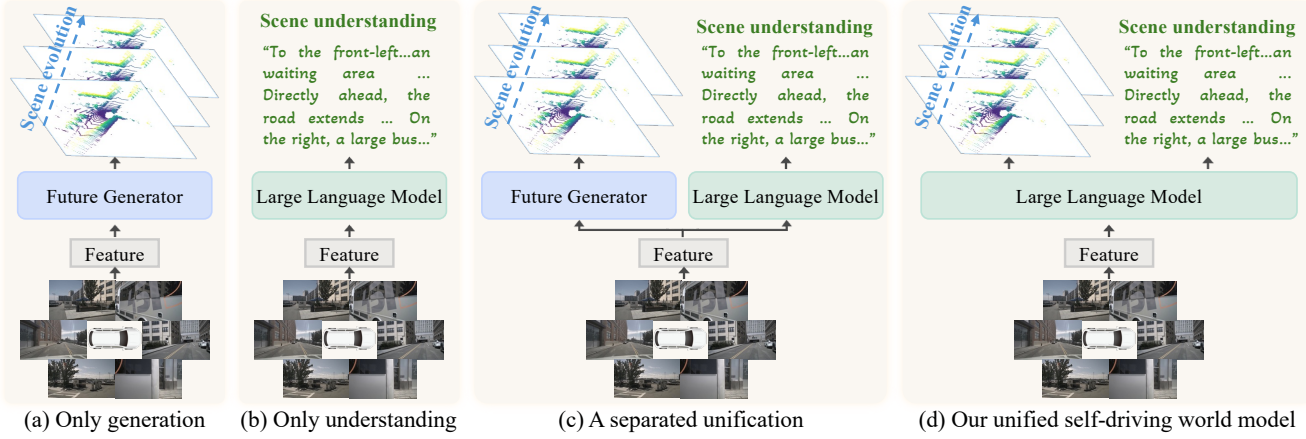


Figure 1. (a) Previous driving world models focus on generative scene evolution prediction. (b) Large language models for driving are limited to scene understanding. (c) A straightforward unification manner using the generator and large language models separately with a shared feature. (d) The proposed simple framework unifies 3D scene understanding and generates scene evolution based on given actions.

Abstract

Driving World Models (DWMs) have become essential for autonomous driving by enabling future scene prediction. However, existing DWMs are limited to scene generation and fail to incorporate scene understanding, which involves interpreting and reasoning about the driving environment. In this paper, we present a unified Driving World Model named **HERMES**. We seamlessly integrate 3D scene understanding and future scene evolution (generation) through a unified framework in driving scenarios. Specifically, HERMES leverages a Bird’s-Eye View (BEV) representation to consolidate multi-view spatial information while preserving geometric relationships and interactions. We also introduce world queries, which incorporate world knowledge into BEV features via causal attention in the Large Language Model, enabling contextual enrichment for understanding and generation tasks. We conduct comprehensive studies on nuScenes and OmniDrive-nuScenes datasets to validate the effectiveness of our method. HERMES achieves

state-of-the-art performance, reducing generation error by 32.4% and improving understanding metrics such as CIDEr by 8.0%. The model and code will be publicly released at <https://github.com/LMD0311/HERMES>.

1. Introduction

Driving World Models (DWMs) [12, 16, 54, 70] have become increasingly important in autonomous driving for their ability to predict future scene evolutions. These models simulate potential changes in the surrounding environment, enabling the vehicles to forecast risk, optimize routes, and make timely decisions in dynamic situations. Among the various modalities, point clouds [15, 24, 28, 65] naturally preserve the geometric relationships between different objects and their surroundings, making them well-suited for accurately describing scene evolutions [22, 57, 67, 76].

However, despite the progress in scene generation, a crucial limitation of current DWMs is their inability to incorporate scene understanding fully. Specifically, while these DWMs excel at predicting how the environment will evolve

* Equal contribution. † Project leader. ✉ Corresponding author.

(Fig. 1(a)), they are hard to interpret and describe the environment, answer questions about it, or provide relevant contextual information (i.e., VQA, scene description).

Recently, vision-language models (VLMs) [6, 27, 31] have achieved remarkable advancements in general vision tasks by leveraging world knowledge and causal reasoning capabilities and have been successfully applied in autonomous driving scenes [44, 50]. As shown in Fig. 1(b), these driving VLMs are capable of performing tasks such as answering complex queries about the driving environment, generating descriptions of scenes, and reasoning about the relationships between various entities. However, while they improve understanding of the current driving environment, they still lack predictive capabilities for how the scene will evolve. This gap limits their effectiveness in autonomous driving, where both 3D scene understanding and future scene prediction are necessary for informed decision-making. This naturally gives rise to the question: *how can world knowledge and future scene evolutions be seamlessly integrated into a unified world model?*

Driven by the above motivation, in this paper, we propose a unified world model that connects both understanding and generation tasks. Our method is referred to as **HERMES**, as illustrated in Fig. 1(d), distinguishes itself from conventional methods, which typically specialize in either generation or scene understanding (e.g., VQA and caption). **HERMES** extends the capabilities of large language models (LLMs) to simultaneously predict future scenes and understand large-scale spatial environments, particularly those encountered in autonomous driving. However, constructing such a unified model is a highly non-trivial problem, as it requires overcoming several key challenges:

Large spatiality in multi-view. LLMs typically face max token length limits, especially in autonomous driving, where multiple surrounding views must be processed (e.g., six-view images in the nuScenes dataset [4]). Directly converting these multi-view images into tokens would exceed the token limit and fail to capture the interactions among different views. To address this, we propose to tokenize the input via a Bird’s-Eye View (BEV) representation. It offers two key benefits: 1) BEV effectively compresses the surrounding views into a unified latent space, thus overcoming the token length limitation while retaining key spatial information. 2) BEV preserves geometric spatial relationships between views, allowing the model to capture interactions between objects and agents across multiple perspectives.

The integration between understanding and generation. A straightforward way to unify scene understanding and generation would be to share the BEV features and apply separate models for understanding (via LLMs) and generation (via a future generator), as presented in Fig. 1(c). However, this approach fails to leverage the potential interactions between understanding and generation. Moreover,

the separate processing of these tasks hinders the optimization process, resulting in suboptimal performance. To address this, we propose to initialize a set of world queries using the raw BEV features (before LLM processing). These queries are then enhanced with world knowledge from text tokens through causal attention in the LLM. As a result, by using the world-knowledge-enhanced queries to interact with the LLM-processed BEV features via a *current to future link*, we ensure that the generated scene evolutions are enriched with world knowledge, effectively bridging the gap between generation and understanding.

By consolidating 3D scene understanding and future scene generation within a single framework, **HERMES** establishes a unified representation that seamlessly accommodates both tasks, offering a holistic perspective on driving environments. This marks a significant step toward a unified DWM, demonstrating the feasibility of integrated driving understanding and generation. Extensive experiments validate the effectiveness of our **HERMES** in terms of both tasks. Notably, our method significantly reduces the error by 32.4% compared to the current state-of-the-art (SOTA) method [65] for generation. Additionally, for the understanding task, our approach outperforms the SOTA [50] by 8.0% under the CIDEr metric on the challenging OmniDrive-nuScenes dataset [50].

Our major contributions can be summarized as follows: **1)** In this paper, we propose **HERMES**, which tames the LLM to understand the autonomous driving scene and predict its evolutions simultaneously. To the best of our knowledge, this is the first world model that can unify the 3D understanding and generation task; **2)** We introduce world queries to capture and integrate world knowledge from text tokens, ensuring that the generated scene evolutions are not only contextually aware but also enriched with world knowledge. This scheme effectively bridges the gap between the understanding and generation tasks, enabling a more coherent and accurate prediction of future scenes.

2. Related Work

World Models for Driving. Driving World Models (DWMs) [14] have gained considerable attention in autonomous driving for obtaining comprehensive environmental representation and predicting future states based on action sequences. Current research mainly focuses on the generation, whether in 2D [35, 53, 73] or 3D [36, 37].

Specifically, most pioneering 2D world models perform a video generation for driving scenarios. GAIA-1 [16] first introduced a learned simulator based on an autoregressive model. Recent work further leverages the large scale of data [21, 63, 68] and more powerful pre-training models, significantly enhancing generation quality regarding consistency [11, 54], resolution [12, 21], and controllability [25, 34, 56, 70]. Concurrently, some studies aim

to generate 3D spatial information for future scenes to provide geometric representations that can benefit autonomous driving systems. Occworld [72] focuses on future occupancy generation and ego planning using spatial-temporal transformers, which has been adapted to other paradigms including diffusion [13, 47], rendering [2, 19, 60], and autoregressive transformer [55]. Additionally, some approaches [22, 57, 67, 76] propose future point cloud forecasting as a world model, among which, ViDAR [65] using images to predict future point clouds through a self-supervised manner.

However, existing DWMs overlook the explicit understanding capacity of the driving environment. This paper aims to propose a unified world model that can both comprehend the scenario and generate scene evolution.

Large Language Models for Driving. Large Language Models (LLMs) exhibit impressive generalization and extensive world knowledge derived from vast data, showcasing remarkable capabilities across various tasks [9, 58, 69]. This has led researchers to explore their applications in autonomous driving, and current studies [8, 38, 43, 52] primarily focus on using LLMs to understand driving scenarios and make perceptual or decision-making outputs. For instance, DriveGPT4 [59] processes front-view video input to predict vehicle actions and provide justifications via an LLM. DriveLM [44] leverages LLMs for graph-based visual question-answering (VQA) and end-to-end driving. ELM [74] enhances the spatial perception and temporal modeling through space-aware pre-training and time-aware token selection. OmniDrive [50] introduces a benchmark with extensive VQA data labeled by GPT-4 [1] and utilizes Q-Former to integrate 2D pre-trained knowledge with 3D spatial. Despite significant advancements and the emergence of various language-based methods, the application of LLMs in driving remains mainly limited to understanding and text modeling. In this paper, we aim to tame the LLM to understand the autonomous driving scene and predict its future evolutions simultaneously.

3. Preliminaries

This section revisits the driving world models and the Bird’s Eye View representation as preliminary.

The Driving World Models (DWMs) seek to learn a general representation of the world from large-scale unlabeled driving data by forecasting future scenarios, enabling the model to grasp the data distribution of real situations. Specifically, given an observation \mathcal{O}_t at time t , the model forecasts information about the next observation \mathcal{O}_{t+1} . The framework of DWMs can be summarized as follows:

$$\mathcal{L}_t = \mathcal{E}(\mathcal{O}_t), \mathcal{L}_{t+1} = \mathcal{M}(\mathcal{L}_t), \mathcal{O}_{t+1} = \mathcal{D}(\mathcal{L}_{t+1}), \quad (1)$$

where \mathcal{E} and \mathcal{D} represent the encoder and decoder for the scene, while the world predictor \mathcal{M} maps the latent state

\mathcal{L}_t to the next time step \mathcal{L}_{t+1} . Together, these components follow the workflow of $\mathcal{O}_t \rightarrow \mathcal{L}_t \rightarrow \mathcal{L}_{t+1} \rightarrow \mathcal{O}_{t+1}$.

Bird’s-Eye View (BEV) has emerged recently as a unified representation offering a natural candidate view. The BEVFormer series [26, 61] exemplifies this approach by leveraging cross-attention to improve 3D-2D view transformation modeling, resulting in robust BEV representations. This BEV feature maintains geometric spatial relationships between views, enabling the model to capture interactions among objects and agents from various perspectives. Additionally, BEV representations are ideal for integrating visual semantics and surrounding geometry, making them well-suited for understanding generation unification.

This paper focuses on unifying the 3D scene understanding and generation by using current multi-view as the observation to generate future point clouds, which inherently maintain accurate geometric relationships among objects and their environments within a BEV-based representation.

4. HERMES

This paper presents HERMES, a unified framework for driving scenarios understanding and generating. Our HERMES serving as a world model that predicts scenes’ point cloud evolution based on image observations and facilitates detailed scene comprehension. The pipeline of our method is illustrated in Fig. 2. We begin with multi-view input images I_t , which are encoded for semantic information using a BEV-based tokenizer and then processed by a Large Language Model (LLM). The LLM predicts the next token based on user instructions to interpret the current autonomous driving scenario. We integrate world queries into the sequence to transfer world knowledge from the conversations to the generation task. The *current to future link* generates future BEV features, and the shared render predicts the current scene point cloud P_t (as an auxiliary task) and generates Δt future scenes from P_{t+1} to $P_{t+\Delta t}$.

4.1. World Tokenizer and Render

The world tokenizer encodes the world observation, i.e., the current multi-view images, into a compressed continuous BEV representation, which is then further processed by the LLM. Conversely, the Render [48, 62, 75] converts BEV features into point clouds to generate geometric information about the scenario. Both modules are detailed as follows.

BEV-based World Tokenizer. To preserve geometric spatial relationships between views and rich semantic information for LLM inputs, we adopt a BEV-based world tokenizer \mathcal{E} . Specifically, the multi-view images I_t at time t are passed through a CLIP image encoder [7, 33] and a single frame BEVFormer v2 [61] without modification. The obtained BEV feature $\mathcal{F}_t^{bev} \in \mathbb{R}^{w \times h \times c}$ captures the semantic and geometric information, where w and h denote the scale of encoded scene, with larger values indicating greater de-

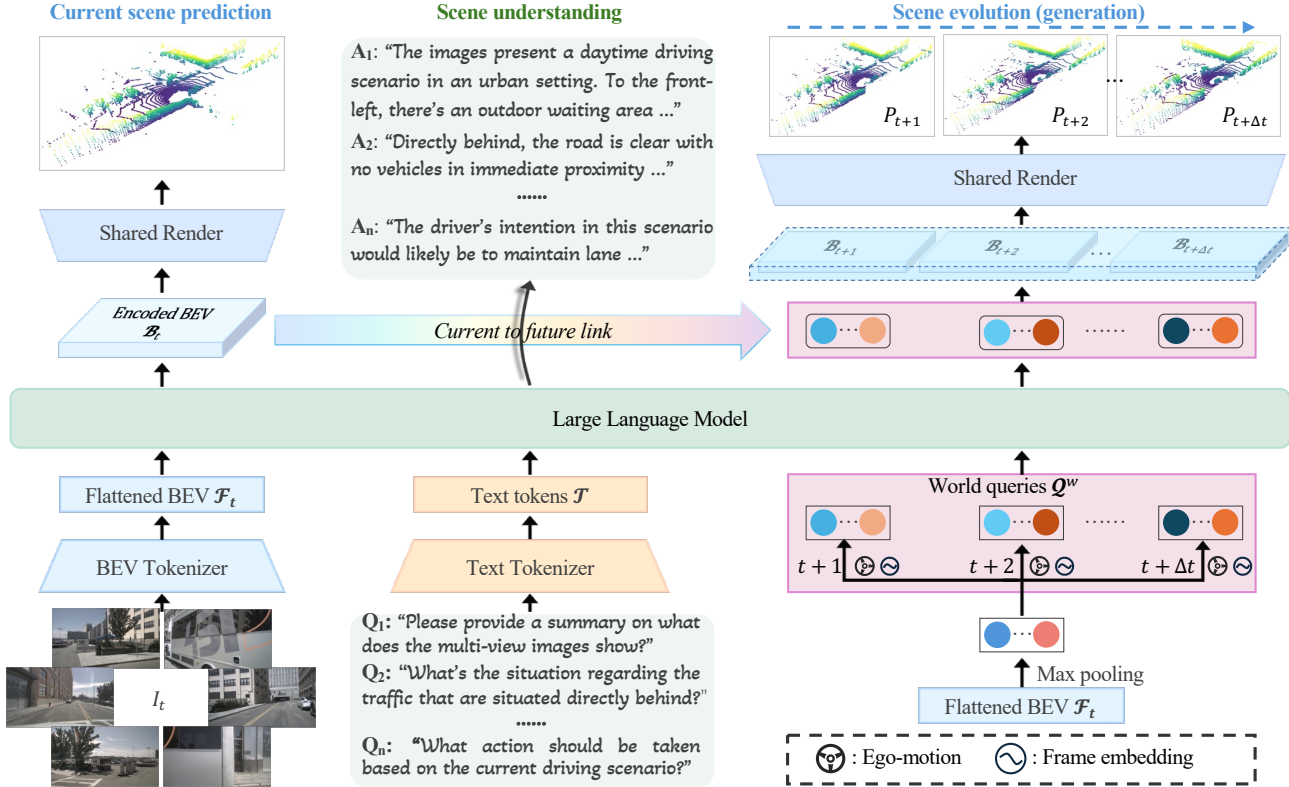


Figure 2. The pipeline of our HERMES. The BEV tokenizer converts multi-view I_t into flattened BEV \mathcal{F}_t , which are fed into the large language model (LLM). The LLM interprets user instructions \mathcal{T} and generates textual responses by leveraging its understanding of driving scenes as world knowledge. A group of world queries \mathcal{Q}^w are appended to the LLM input sequence. Encoded BEV \mathcal{B}_t and world queries generate future BEV ($\mathcal{B}_{t+1}, \dots, \mathcal{B}_{t+\Delta t}$) via a *current to future link*, and the shared Render generates point clouds evolution.

tail, and c is the channel dimension of BEV. However, such a feature, often containing tens of thousands of tokens, is too large for the LLM [66]. To address this, we implement a down-sampling block that reduces \mathcal{F}_t^{bev} by two times, resulting in a compressed shape of $\mathbb{R}^{\frac{w}{4} \times \frac{h}{4} \times (c \times 4)}$. When the LLM is required, the down-sampled feature will be flattened and projected to $\mathcal{F}_t \in \mathbb{R}^{L_{bev} \times C}$, where $L_{bev} = \frac{w}{4} \times \frac{h}{4}$.

BEV-to-Point Render. We introduce a simple BEV-to-Point Render \mathcal{R} , aiming to map the aforementioned down-sampled feature to the scene point cloud P_t . Specifically, we first up-sample the compressed BEV feature (or encoded BEV $\mathcal{B}_t \in \mathbb{R}^{L_{bev} \times (c \times 4)}$ after processing of the LLM and an out-projection) to the shape of $\mathbb{R}^{w \times h \times c}$ using nearest neighbor interpolation and convolutions. To address the absence of height information in the BEV feature, we reshape the input to $\mathbb{R}^{w \times h \times z \times \frac{c}{z}}$ by adding an extra height dimension. We then apply a series of 3D convolutions to reconstruct the volumetric feature $\mathcal{F}_t^{vol} \in \mathbb{R}^{w \times h \times z \times c'}$, where z is the height and c' is the output channel dimension. Finally, we construct rays $\{\mathbf{r}_k\}_{k=1}^K$ according to the LiDAR setup of the dataset and use differentiable volume rendering to compute the depth for each ray.

The rendering process models the environment as an im-

plicit signed distance function (SDF) field to capture intricate geometric details accurately [48, 62, 75]. Given a ray \mathbf{r}_k originating from \mathbf{o} and directed along \mathbf{t}_k , we discretize it into n sampled points $\{\mathbf{p}_i = \mathbf{o} + d_i \mathbf{t}_k \mid i = 1, \dots, n \text{ and } 0 \leq d_i < d_{i+1}\}$, where \mathbf{p}_i corresponds to a location in 3D space, determined by its depth d_i along the ray. For each sampled point, we retrieve a local feature embedding \mathbf{f}_i from the volumetric representation \mathcal{F}_t^{vol} via trilinear interpolation. Subsequently, a shallow MLP ϕ_{SDF} is used to predict the SDF value $s_i = \phi_{SDF}(\mathbf{p}_i, \mathbf{f}_i)$. With the predicted SDF values, the rendered depth $\tilde{d}(\mathbf{r}_k)$ is computed through a weighted integration of all sampled depths by $\tilde{d}(\mathbf{r}_k) = \sum_{i=1}^n w_i d_i$, where $w_i = T_i \alpha_i$ [48] represents an unbiased, occlusion-aware weight. The transmittance $T_i = \prod_{j=1}^{i-1} (1 - \alpha_j)$ accumulates the survival probability of photons up to the j -th sample, $\alpha_i = \max\left(\frac{\sigma_t(s_i) - \sigma_t(s_{i+1})}{\sigma_t(s_i)}, 0\right)$ indicates the opacity, and $\sigma_t(x) = (1 + e^{-tx})^{-1}$ is a sigmoid modulated by a learnable parameter t .

4.2. Unification

This section introduces the unification of world understanding and future scene generation within our HERMES. The Large Language Model (LLM) interprets driving scenarios

from world tokenizer outputs (\mathcal{F}_t) based on user instructions. Δt groups of world queries gather knowledge from conversations, aiding in generating scene evolution.

Large Language Model. As shown in Fig. 2, the LLM is pivotal to our HERMES, modeling BEV inputs \mathcal{F}_t , parsing user instructions, acquiring world knowledge from real driving scenario inquiries, and generating predictions. We utilize the LLM within the widely used InternVL2 [5].

Understanding. Following prior work [31, 32], we project the flattened BEV to a shape of $\mathbb{R}^{L_{bev} \times C}$ and into the feature space of the LLM using a two-layer MLP, where L_{bev} is the input BEV length, and C is the channel dimension of LLM. For prompts on the current scene, we tokenize them into distinct vocabulary indices and text tokens \mathcal{T} for processing by the LLM. Like existing multi-modal language models [5, 27], HERMES responds to user queries about the driving environment, providing scene descriptions and answers to visual questions. The LLM understands the scene through a next-token prediction approach.

Generation. Predicting and generating future changes based on observations of the current moment requires the model to have an exhaustive understanding of the world. To endow the LLM with future-generation capability, we propose a world query technique, which links world knowledge to future scenarios and improves information transfer between the LLM and the Render. As in Fig. 2, we outline the generation process in terms of LLM input and output.

For the input to the LLM, we utilize Δt groups of world queries $\mathcal{Q}^w \in \mathbb{R}^{(\Delta t \times n) \times C}$, where n is the number of queries per group and C represents the channel dimension of LLM. We emphasize the importance of proper feature initialization for effective learning. Thus, we employ a max pooling to derive the world queries from the peak of the BEV feature \mathcal{F}_t , yielding $\mathcal{Q} \in \mathbb{R}^{n \times (c \times 4)}$. The \mathcal{Q} is then copied Δt times as query groups $\{\mathcal{Q}_i | i = 1, \dots, \Delta t\}$. To further enable controllable future generation, we encode the ego-motion condition to e_{t+i} , which describes the planned future positions and heading of the ego-vehicle from the current to the i -th frame into high-dimensional embeddings. The ego-motion information e_{t+i} is then added to the corresponding queries \mathcal{Q}_i . Additionally, a frame embedding $FE \in \mathbb{R}^{\Delta t \times (c \times 4)}$ is incorporated by the broadcast mechanism to denote the prediction frames for which group of world queries is responsible. The world queries \mathcal{Q}^w and flattened BEV \mathcal{F}^t share the language-space projection layer (i.e., MLP) to project from $c \times 4$ to C for the language model channel. The $\mathcal{Q}^w \in \mathbb{R}^{(\Delta t \times n) \times C}$ can be computed as:

$$\mathcal{Q}^w = \text{MLP}(\text{Concat}[\mathcal{Q}_i + e_{t+i} | i = \{1, \dots, \Delta t\}] + FE). \quad (2)$$

The LLM’s causal attention mechanism (i.e., the later token can access the earlier information) allows world queries to access world knowledge derived from the understanding process. After being processed by the LLM feed-forwardly,

the encoded BEV feature and world quires are projected by a shared two-layer MLP from the channel dimension of LLM C back to the channel of $c \times 4$. Note that each group of world queries contains only n queries, which provide a sparse view of the future world, complicating the reconstruction of the future scene by the world Render. To address this, we propose the *current to future link* module, which employs cross-attention layers to inject world knowledge for future BEV features. Specifically, the *current to future link* module contains 3 cross-attention blocks for generating future BEV features. Each cross-attention block includes a cross-attention layer that uses the encoded BEV \mathcal{B}_t from the LLM output as the query, with world queries for each scene serving as the value and key. A self-attention layer and a feed-forward network further process spatial information. The encoded BEV (\mathcal{B}_t) and generated future BEV features ($\mathcal{B}_{t+1}, \dots, \mathcal{B}_{t+\Delta t}$) are sent to a shared world Render and obtain point cloud from P_t to $P_{t+\Delta t}$.

4.3. Training Objectives

To perform auto-regressive language modeling, we employ Next Token Prediction (NTP) to maximize the likelihood of text tokens, following the standard language objective:

$$\mathcal{L}_N = - \sum_{i=1} \log P(\mathcal{T}_i | \mathcal{F}_t, \mathcal{T}_1, \dots, \mathcal{T}_{i-1}; \Theta), \quad (3)$$

where $P(\cdot | \cdot)$ represents the conditional probability modeled by the weights Θ , \mathcal{F}_t is the flattened BEV feature for the input frame, and \mathcal{T}_i denotes the i -th text token.

For point cloud generation, we supervise the depths of various rays $d(\mathbf{r}_k)$ using only L1 loss:

$$\mathcal{L}_D = \sum_{i=0}^{\Delta t} \lambda_i \frac{1}{N_i} \sum_{k=0}^{N_i} |d(\mathbf{r}_k) - \tilde{d}(\mathbf{r}_k)|, \quad (4)$$

where λ_i is the loss weight for frame $t + i$, and N_i is the number of rays in the point clouds for frame $t + i$. The total loss for HERMES is given by $\mathcal{L} = \mathcal{L}_N + 10\mathcal{L}_D$.

5. Experiments

5.1. Dataset and Evaluation Metric

Datasets. 1) **NuScenes** [4] is a widely used autonomous driving dataset, which includes 700 training scenes, 150 validation scenes, and 150 test scenes. We use six images and the point clouds captured by surrounding cameras and the LiDAR, respectively. 2) **NuInteract** [71] is a newly proposed language-based driving dataset with dense captions for each image and scene. With $\sim 1.5M$ annotations, it supports various tasks, such as 2D perception and 3D visual grounding. 3) **OmniDrive-nuScenes** [50] supplements nuScenes with high-quality caption and visual question-answering (QA) text pairs generated by GPT4. Considering

Table 1. The comparison of our HERMES and understanding/generation specialist models. L/C/T refers to LiDAR/camera/text, respectively. We report MTETOR, CIDEr, and ROUGE for understanding tasks, and Chamfer distance for 0-3s on the (OmniDrive-)nuScenes validation set, following ViDAR [65]. [†] denotes results from ViDAR, while scores for GPT-4o and LLaVA-OV are sourced from DriveMM [18].

Method	Reference	# LLM Params	Modality	Generation				Understanding		
				0s ↓	1s ↓	2s ↓	3s ↓	MTETOR ↑	ROUGE ↑	CIDEr ↑
<i>Only Generation</i>										
4D-Occ [†] [22]	CVPR 23	-	L→L	-	1.13	1.53	2.11	Unsupported	0.223	0.244
ViDAR [65]	CVPR 24	-	C→L	-	1.12	1.38	1.73			
<i>Only Understanding</i>										
GPT-4o [20]	-	-	C→T	Unsupported				-	0.223	0.244
LLaVA-OV [23]	arXiv 24	7B	C→T	Unsupported				-	0.221	0.284
OmniDrive [50]	CVPR 25	7B	C→T	Unsupported				0.380	0.326	0.686
OmniDrive-2D [50]	CVPR 25	7B	C→T	Unsupported				0.383	0.325	0.671
OmniDrive-BEV [50]	CVPR 25	7B	C→T	Unsupported				0.356	0.278	0.595
<i>Unified Understanding and Generation</i>										
Separated unification	-	1.8B	C→T&L	0.60	0.84	1.08	1.37	0.384	0.327	0.745
HERMES (ours)	-	1.8B	C→T&L	0.59	0.78	0.95	1.17	0.384	0.327	0.741

the high quality and rich VQA annotations, we perform the understanding training and evaluation on the OmniDrive-nuScenes description and conversation data.

Evaluation Metric. For understanding tasks, we utilize widely used METEOR [3], CIDEr [46], and ROUGE [29] metrics to compute similarities between generated and ground-truth answers at the word level. For generation evaluation, we follow previous work [65] and use Chamfer Distance to measure precision in generated point clouds, considering only points within the range of [-51.2m, 51.2m] on the X- and Y-axes, and [-3m, 5m] on the Z-axis.

5.2. Main Results

We compare HERMES with understanding [20, 23, 50] and generation [22, 65] specialist models in Tab. 1, which demonstrates competitive performance on both tasks and promote strong unification.

For future point cloud generation, both 4D-Occ and ViDAR utilize a 3s history horizon, while our HERMES only relies on the current frame, achieving significant improvements. Remarkably, with only multi-view inputs, HERMES is capable of generating a more accurate representation of the scene geometry for predicting future evolution, resulting in $\sim 32\%$ Chamfer Distance reduction in 3s point clouds compared to ViDAR. It should be noted that ViDAR utilizes a carefully designed latent render and an FCOS3D [51] pre-trained backbone, while HERMES uses simple volumetric representation. Furthermore, HERMES can simultaneously understand the current scenario, which is a crucial capability for driving systems but is challenging for existing driving world models.

For 3D scene understanding, we continuously achieve highly competitive results in caption quality compared to understanding specialists. For example, we notably outperform OmniDrive by 8% on the CIDEr metric and excel in

MTETOR and ROUGE. Note that OmniDrive leverages extensive 2D pre-training data [10], supervision from 3D objects [49], and lane detection. The OmniDrive-BEV uses LSS [40] to transform perspective features into a BEV feature and SOLOFusion [39] for temporal modeling. While it utilizes a BEV representation, its scene understanding is limited, likely due to insufficient data for BEV-based image-text alignment. Further compared to the Separated unification model, our unified approach yields significantly better generation results while maintaining strong understanding performance. This demonstrates successful cross-task knowledge transfer and consistent scene modeling within our compact, unified HERMES.

5.3. Ablation Study

Unless otherwise specified, we perform ablation studies trained on a quarter of the nuScenes training scenes. Default settings are marked in green.

Analysis on understanding and generation interaction. Our HERMES achieves a strong and seamless unification of understanding and generation in driving scenes. We first analyze the relationship between these two processes. As shown in Tab. 2, we conduct experiments with four approaches: solely understanding, solely generation, a separated unification, and our method. The separated unification involves sharing the flattened BEV while using separate models for understanding and generation, as in Fig. 1(c). We find that HERMES achieves highly competitive results compared to training on one task, with a minor performance gap (e.g., 0.002 difference on MTETOR/ROUGE and a 0.03 chamfer distance gap on the 3s generation). Nevertheless, our approach shows better results at 0-1s, indicating ongoing optimization challenges in the unified understanding and generation stage. Ultimately, our HERMES outperforms the separated unification in generation results, as the lat-

Table 2. Ablation on interaction of tasks.

Under.	Gen.	Generation				Understanding		
		0s ↓	1s ↓	2s ↓	3s ↓	MTETOR ↑	ROUGE ↑	CIDEr ↑
✓	-	-	-	-	-	0.379	0.323	0.728
-	✓	0.651	0.988	1.313	1.687	-	-	-
Separated	unify	0.663	1.095	1.476	1.875	0.377	0.321	0.722
✓	✓	0.645	0.984	1.333	1.718	0.377	0.321	0.720

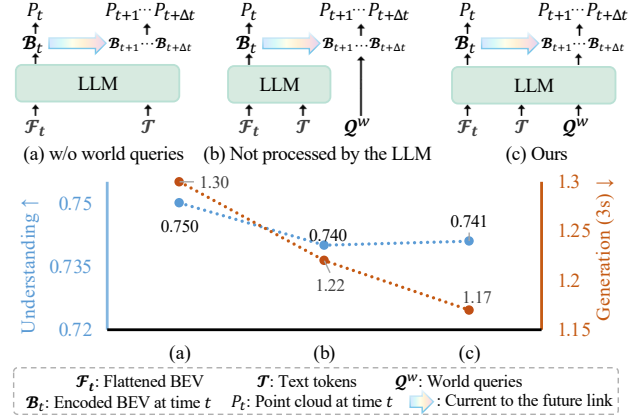


Figure 3. The effect of world queries for understanding (CIDEr) and generation (3s chamfer distance) is trained on full data.

ter fails to exploit the potential interactions between understanding and generation, and the separation hinders optimization and leads to suboptimal performance.

Analysis on the effect of the world queries. We then validate the efficacy of world queries (Q^w), as shown in Fig. 3. Without world queries (Fig. 3(a)), the sequences $\mathcal{B}_{t+1}, \dots, \mathcal{B}_{t+\Delta t}$ are generated by directly integrating future ego motion into \mathcal{B}_t . It can be found that introducing world queries significantly improves future generation capabilities, reducing the Chamfer Distance for 3s point cloud prediction by 10%. Although there is a slight 1% decrease in understanding performance (CIDEr), we attribute this to the increased optimization complexity from adding new informational parameters to the LLM. A comparison of Fig. 3(b)-(c) further reveals that Q^w processed through the LLM enhances generative performance, supporting their role in effective world knowledge transfer.

Analysis on generation length. In Tab. 3, we discuss the number of generated frames for future scenes. As the number increases, the generation results exhibit a slight drop, which we attribute to an optimization dilemma within the LLM. This suggests that a more efficient interaction method could be explored in the future. Additionally, we evaluate the auxiliary role of current point cloud prediction for future generation, as shown in the last two rows of Tab. 3. Predicting the current frame regularizes the encoded BEV (\mathcal{B}_t) from the LLM outputs, enhancing future generation results. More importantly, training for current point cloud

Table 3. Ablation on generation length.

Second	Generation				Understanding						
	0	1	2	3	0s ↓	1s ↓	2s ↓	3s ↓	MTETOR ↑	ROUGE ↑	CIDEr ↑
✓	✓	-	-	-	0.607	0.944	-	-	0.379	0.323	0.725
✓	✓	✓	-	-	0.632	0.951	1.313	-	0.378	0.321	0.714
-	✓	✓	✓	-	1.078	1.397	1.779	-	0.378	0.321	0.717
✓	✓	✓	✓	-	0.645	0.984	1.333	1.718	0.377	0.321	0.720

Table 4. Ablation on the source of world queries.

pooling	Generation				Understanding		
	0s ↓	1s ↓	2s ↓	3s ↓	MTETOR ↑	ROUGE ↑	CIDEr ↑
Attn.	0.656	1.001	1.344	1.748	0.377	0.321	0.712
Avg.	0.660	0.996	1.348	1.741	0.376	0.321	0.715
Max	0.645	0.984	1.333	1.718	0.377	0.321	0.720

Table 5. Ablation on size for the flattened BEV.

BEV size	Generation				Understanding		
	0s ↓	1s ↓	2s ↓	3s ↓	MTETOR ↑	ROUGE ↑	CIDEr ↑
25 × 25	0.720	1.040	1.347	1.698	0.367	0.311	0.671
50 × 50	0.645	0.984	1.333	1.718	0.377	0.321	0.720

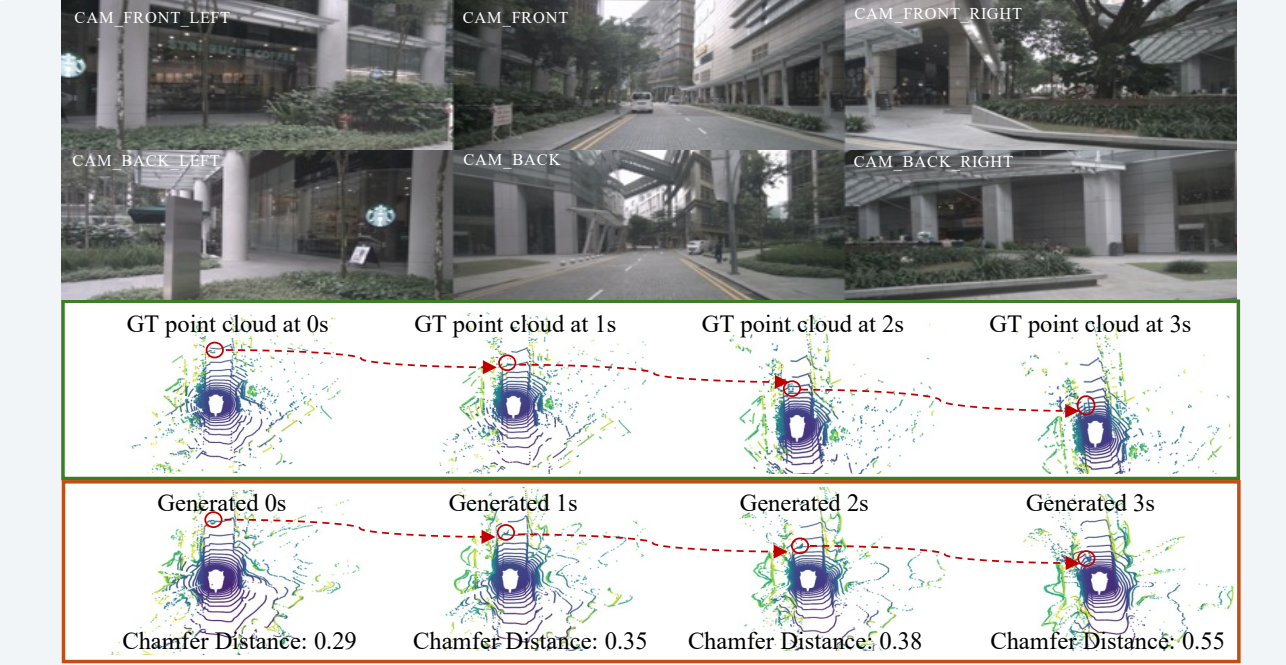
prediction does not add extra inference burden for future generations, serving as a practical auxiliary task.

Analysis on the source of world queries. We also assess the initialization of world queries in Tab. 4, including attention pooling [42, 45], adaptive average pooling and max pooling. It shows that world queries derived from the adaptive max pool of the flattened BEV \mathcal{F}_t perform better in Chamfer Distance on 3s. We argue that the max pool effectively captures peak responses from \mathcal{F}_t , whereas average or attention pooling may overly emphasize global information, potentially affected by background noise.

Analysis on the size of flattened BEV. We finally analyze the impact of flattened BEV (\mathcal{F}_t) size by varying the BEV tokenizer’s downsampling multiplier, resulting in different feature lengths. Experiments with 8 \times and 4 \times downsampling yield \mathcal{F}_t with spatial resolutions of 25 and 50, respectively. Tab. 5 demonstrates that a spatial size of 50 \times 50 significantly improves CIDEr and 0s generation by 7.3% and 10% compared to 25 \times 25. We attribute this improvement to reduced information loss compared to excessive downsampling, enhancing text comprehension and facilitating point cloud recovery/prediction. While further increasing the size of \mathcal{F}_t might improve performance, we chose 50 \times 50 as a trade-off due to LLM processing length limitations.

5.4. Qualitative Results

This section presents qualitative results on future generations and scene understanding, as illustrated in Fig. 4. Our



Q: Can you provide a summary of the current driving scenario based on the input images?

A: The vehicle is currently navigating through an urban environment, seemingly a **business district** with modern architecture and office buildings. **On the left**, the view is dominated by a **Starbucks Coffee** shop with a large **glass facade** and a **lush greenery barrier**, while **on the right**, an open plaza with more green spaces and **seated areas** suggests a pedestrian-friendly zone. The road ahead is clear, marked with well-defined lane lines, and there are no visible traffic signals or signs indicating any immediate need to stop or yield. The weather appears overcast, providing soft lighting without the glare of direct sunlight. Looking behind, the street is equally clear, with **no vehicles or pedestrians in close proximity**, indicating a low traffic condition.

Q: Is there a traffic signal in sight that the vehicle should be aware of?

A: **No**, there is **no traffic signal** visible in the front or rear views that the vehicle should be aware of at this moment.

Q: Are there any pedestrians close to the vehicle's path?

A: **No**, there are **no pedestrians close to the vehicle's path** on the sidewalks or crossing the streets.

Q: Can you see any vehicles in your rearview that you should be aware of?

A: The rear view is **clear of any close following vehicles**, allowing for a comfortable driving distance.

Q: Is there any oncoming traffic that might affect your driving?

A: There is **no oncoming traffic visible** that would affect the current driving conditions.

Q: What action should be taken in the current driving scenario?

A: Given the clear road ahead and the current driving conditions, the vehicle should maintain a moderate speed and stay in the current lane. **In-** Continue to monitor the surroundings for any unexpected pedestrians that may enter the roadway from the right side where the pedestrian plaza is located. **In-** Regularly check the rearview and side mirrors to stay aware of any vehicles that may approach from behind, although the current rear view shows no immediate traffic. **In-** Be prepared to react to any traffic signals or signs that may come into view, even though none are currently visible.

Figure 4. Qualitative results for future generation and scene understanding. From top to bottom, we display the multi-view input of the current scene, the ground truth scene evolution, the generated scene evolution, and the scene understanding result.

HERMES effectively captures future scene evolution, such as the van keeping close to the ego vehicle, noted in the red circle. Furthermore, HERMES exhibits a strong understanding of BEV inputs, as indicated by the green text, accurately identifying objects such as “Starbucks”.

6. Conclusion

This paper introduces **HERMES**, a simple yet effective unified Driving World Model that integrates 3D scene understanding and future scene generation within a single framework. We effectively bridge the gap between understanding and generation by leveraging a Bird’s-Eye View representation and incorporating world queries enhanced through

large language models. Extensive experiments validate the effectiveness of the proposed HERMES, demonstrating significant improvements in future scene prediction accuracy and understanding metrics. We believe this work is a significant step toward a stronger unified Driving World Model.

Limitation. Although HERMES achieves promising results in unifying 3D scene understanding and generation, there are some limitations: 1) We have not explored perception tasks for autonomous driving within our framework. 2) Future image is also an important generation modality but is still under exploration. We left these in our future work.

Acknowledgment. This work was supported by the NSFC (62225603, 62441615, and 623B2038).

HERMES: A Unified Self-Driving World Model for Simultaneous 3D Scene Understanding and Generation

Supplementary Material

S1. Additional Experiments

S1.1. Training Details

The BEV-based tokenizer utilizes the OpenCLIP ConNext-L backbone [7, 33, 42], while other modules in the tokenizer and Render are trained from scratch. The LLM is derived from InternVL2-2B [5, 6]. The resolution of the input image is 1600×900 , while the BEV-based world tokenizer adopts the same hyperparameters as BEVFormer v2-base [61], with the size of the encoded scene set to $w = h = 200$ and a BEV channel dimension of 256. The z and c' in the BEV-to-point clouds Render are set to 32. For future generation, we forecast scene evolution over 3 seconds, i.e., $\Delta t = 3$. The frame-wise weights in Eq. 4 of the main paper are empirically defined by $\lambda_i = 1 + 0.5 \times i$, $i \in \{0, \dots, 3\}$, corresponding to the point clouds from 0 to 3s. The training of HERMES is structured into three stages and detailed below. Additional details are provided in Tab. S1.

Stage-1: Tokenizer Training. In initial stage, we train the world tokenizer \mathcal{E} and Render \mathcal{R} to convert current images (I_t) into point clouds (P_t), following $P_t = \mathcal{R}(\mathcal{E}(I_t))$. We utilize 12Hz data from the nuScenes training set for the tokenizer and Render learning.

Stage-2: BEV-Text Alignment and Refinement. This stage encompasses BEV-Text alignment and refinement tuning phases. The alignment phase aims to establish vision-language alignment between the input and output BEV of the LLM, training only the in-projections for flattened BEV embeddings and out-projections for the encoded BEV. To alleviate data deprivation, we propose a simple data augmentation involving masking one of the multi-view images, splicing the caption from the visible view, and using the unprocessed multi-view scene descriptions. This approach increases the multi-view image-text pairs to $\sim 200K$, a sevenfold increase from the nuScenes keyframes. In the refinement phase, all parameters are unfrozen, and the LLM is fine-tuned using LoRA [17]. The alignment phase employs NuInteract [71] dense caption data, while the refinement phase adapts labeling styles using scene description data from OmniDrive-nuScenes [50].

Stage-3: Understanding and Generation Unification. Building on the understanding gained in the first two stages, we introduce future generation modules to generate point clouds at different moments. We train using nuScenes keyframes, descriptions, and general conversation annotations from OmniDrive-nuScenes.

Table S1. Training details of HERMES. -/- in Stage 2 indicates BEV-text alignment/refinement.

Config	Stage 1	Stage 2	Stage 3
Optimizer	AdamW	AdamW	AdamW
Learning Rate	2e-4	2e-4/4e-4	4e-4
Training Epochs	6	3/6	36
Learning Rate Scheduler	Cosine	Cosine	Cosine
Batch Size Per GPU	1	4	4
GPU Device		32×NVIDIA H20	

Table S2. Ablation on scaling potential of the LLM.

# LLM Params	Generation				Understanding		
	0s ↓	1s ↓	2s ↓	3s ↓	MTETOR ↑	ROUGE ↑	CIDEr ↑
0.8B	0.668	1.015	1.379	1.809	0.372	0.318	0.703
1.8B	0.645	0.984	1.333	1.718	0.377	0.321	0.720
3.8B	0.643	0.991	1.321	1.701	0.381	0.325	0.730

Table S3. Ablation on the number n of world queries.

n	Generation				Understanding		
	0s ↓	1s ↓	2s ↓	3s ↓	MTETOR ↑	ROUGE ↑	CIDEr ↑
1	0.658	0.996	1.328	1.725	0.376	0.320	0.712
2	0.656	0.995	1.324	1.720	0.377	0.321	0.714
4	0.645	0.984	1.333	1.718	0.377	0.321	0.720
8	0.667	1.028	1.361	1.744	0.376	0.321	0.713
16	0.658	0.999	1.354	1.748	0.378	0.321	0.716

S1.2. Additional Ablation Study

Unless otherwise specified, we perform ablation studies trained on a quarter of the nuScenes training scenes. Default settings are marked in green.

Analysis on the scaling potential of the LLM. We first explore the scaling potential of our HERMES, as shown in Tab. S2. Scaling up LLMs yields consistent gains in 3D scene understanding and point cloud generation, and we utilize the 1.8B LLM from InternVL2-2B [5, 6] as a trade-off. This indicates that the broader world knowledge acquired during pre-training enhances these tasks, suggesting potential benefits from further scaling.

Analysis on the number of world queries. The world queries facilitate knowledge transfer between the LLM and the Render for future scenarios. We then evaluate the impact of the number of queries n for each group, as shown in Tab. S3. We find that world queries do not adversely affect text understanding quality. However, increasing the

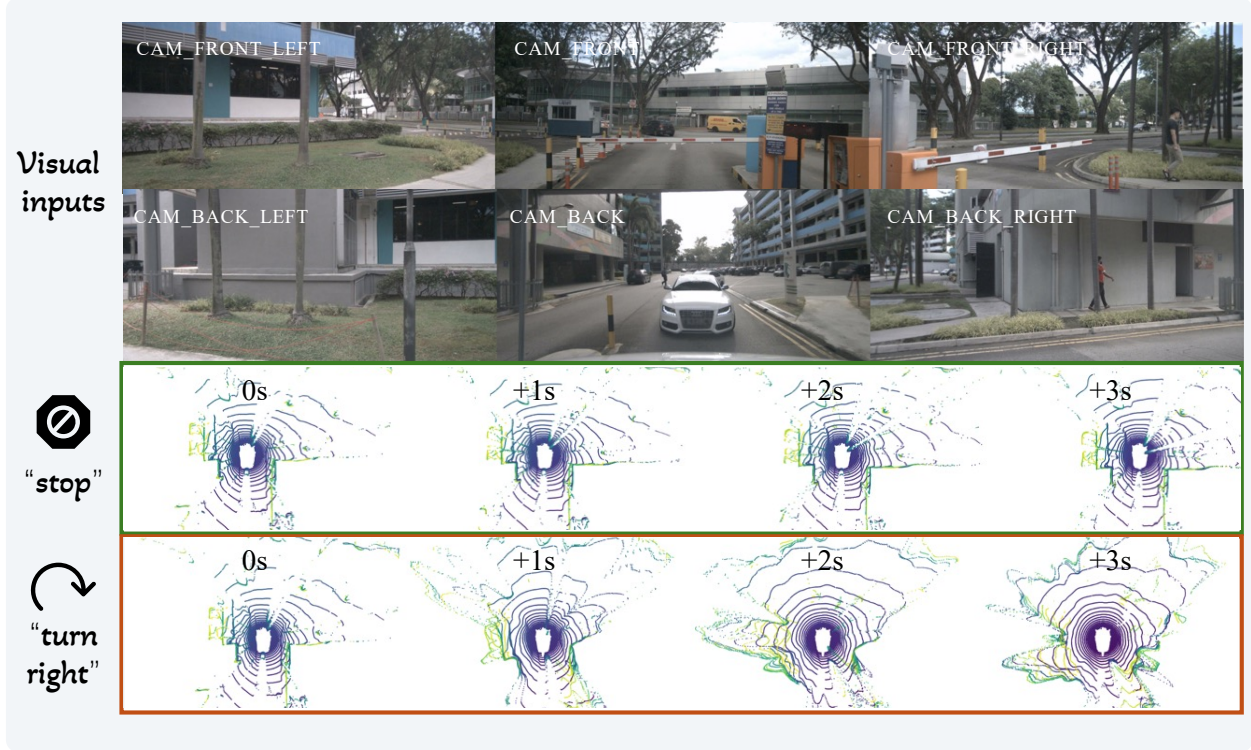


Figure S1. Qualitative results of HERMES conditioned on different future ego-motion conditions. From top to bottom, each sub-figure displays the multi-view input of the current scene, scene evolution predicted with a “stop” future ego-motion, and scene evolution predicted with a “turn right” ego-motion.

Table S4. Comparison of generation ability.

	Generation				Understanding		
	0s ↓	1s ↓	2s ↓	3s ↓	MTETOR ↑	ROUGE ↑	CIDEr ↑
Copy&Paste	-	1.27	2.12	2.66	-	-	-
ViDAR [65]	-	1.12	1.38	1.73	-	-	-
HERMES	0.59	0.78	0.95	1.17	0.384	0.327	0.741

Table S5. VQA results on NuScenes-QA.

Method	Reference	Modality	Acc. (%) ↑
LLaVA [30]	NeurIPS 23	Camera	47.4
LiDAR-LLM [64]	arXiv 23	LiDAR	48.6
BEVDet+BUTD [41]	AAAI 24	Camera	57.0
BEVDet+MCAN [41]	AAAI 24	Camera	57.9
CenterPoint+BUTD [41]	AAAI 24	LiDAR	58.1
CenterPoint+MCAN [41]	AAAI 24	LiDAR	59.5
OmniDrive [50]	CVPR 25	Camera	59.2
HERMES	-	Camera	61.9

number of world queries leads to a decline in performance, likely due to redundant information and optimization challenges. Therefore, we choose to include four world queries per group for future generations.

Analysis on generation ability. We finally compare our future point cloud generation ability trained on the full train-

ing set against a Copy&Paste baseline, where Copy&Paste simply duplicates the current ground-truth point cloud for future observations. As shown in Tab. S4, this baseline fails to account for point cloud changes due to movement and occlusion, demonstrating that HERMES truly learns to understand 3D scenes and predict their future evolution.

S1.3. Understanding on NuScenes-QA

The NuScenes-QA [41] is another multi-modal VQA benchmark for driving scenarios, featuring primarily single-word answers focused on perception. We fine-tune HERMES on the NuScenes-QA training set to align with its style and length, and the results are shown in Tab. S5. HERMES achieves superior performance, outperforming LLaVA [30] by 14.5% and the point cloud method CenterPoint+MCAN [41] by 2.4%. This showcases HERMES’s strong 3D scene understanding capabilities via its unified BEV representation, especially considering it requires no 3D object detection supervision.

S2. Discussion

The integration of Bird’s-Eye View (BEV) representations as input for Large Language Models (LLMs) presents distinct advantages in our HERMES. Unlike conventional multi-view processing approaches that process individual

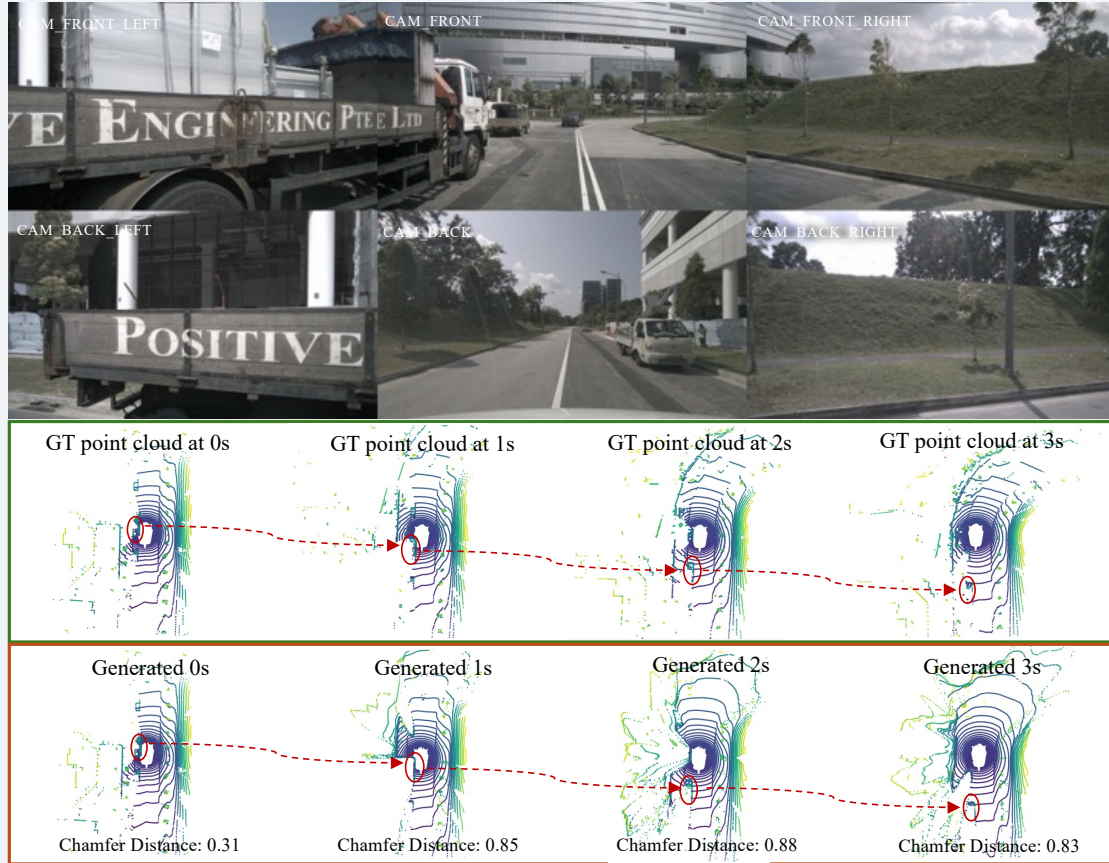
camera streams independently, the BEV-based tokenization establishes a unified spatial coordinate system that inherently preserves geometric relationships across views while maintaining object interaction patterns. This spatial consolidation addresses the inherent limitations of vision-language models in interpreting multi-perspective scenarios, where disconnected 2D projections fail to capture the holistic 3D environment context. By strategically compressing high-resolution multi-view inputs (1600×900 per view, for example) into a compact BEV latent space through our downsampling block, we achieve efficient token utilization (2,500 tokens vs. ~47,000 tokens for raw view processing) without exceeding standard LLM context windows. Crucially, the spatial-aware BEV features enable synergistic knowledge transfer between scene understanding and generation tasks through our world query mechanism, i.e., the positional correspondence between text descriptions and geometric features permits causal attention patterns that enrich future predictions with linguistic context. Our experiments on nuScenes demonstrate that this spatial-textual alignment contributes substantially to the 32.4% reduction in generation error and 8.0% CIDEr improvement, validating BEV’s dual role as both information compressor and cross-modal interface.

S3. More Qualitative Results

This section presents further qualitative results of HERMES on controllability and the unification ability of understanding and generation.

Potential for Controlled Scene Generation. As shown in Fig. S1, we observe the capability of HERMES to generate future point cloud evolution conditioned on specific ego-motion information, such as “stop” or “turn right”. This showcases the potential of HERMES as world simulator and its ability to understand complex world scenarios deeply.

Unification of understanding and generation. More qualitative results on future generations and scene understanding are illustrated in Fig. S2. Our HERMES effectively captures future scene evolution (with the ground truth ego-motion information for better comparison), such as the corner of the building keeps moving backward, noted in the red circle in Fig. S2b. While HERMES achieve an encouraging integration of understanding and generation, it faces challenges in complex scenes (e.g., significant left turns and occlusions as in Fig. S2a) and low-quality visible light conditions (e.g., nighttime driving as in Fig. S2c). Despite the complexity of the scenarios, HERMES still makes reasonable predictions about the emerging parts of future scenes.



Q: Can you provide a summary of the current driving scenario based on the input images?

A: The vehicle is positioned on a clear, marked road during what appears to be daytime with good visibility and dry weather conditions. To the left, there's a **stationary construction vehicle**, indicating potential work nearby or a temporary halt in traffic. Straight ahead, the road is free of obstructions with a few vehicles at a distance, suggesting a smooth flow of traffic. The road is bordered by **greenery on both sides**, with a **grassy slope to the right** and trees lining the road, contributing to a serene driving environment. In the rear view, there are **no vehicles closely following**, providing a sense of ease for potential maneuvers. The overall scene suggests a non-congested urban or suburban setting with minimal traffic activity.

Q: Is there a traffic signal or stop sign visible?

A: **No**, there is no traffic signal or stop sign visible in the current view.

Q: What type of vehicles are visible in the current driving scene?

A: There is a **construction vehicle on the left side** and a white SUV on the right side of the road.

Q: Are there any pedestrians or cyclists on the road?

A: **No**, there are **no pedestrians** or cyclists visible on the road in the current view.

Q: What is the condition of the road surface?

A: The road surface appears to be in good condition, with **clear lane markings and no visible potholes or debris**.

Q: Are there any indications of construction work or road maintenance?

A: The presence of the **construction vehicle and the fenced-off area to the left** suggest **ongoing construction or maintenance work**.

Q: How would you describe the driving conditions based on the weather?

A: The driving conditions seem to be favorable, with **clear weather and daylight** providing good visibility.

Q: Based on the surroundings, what kind of area is the vehicle driving through?

A: The vehicle is driving through an urban area with **modern buildings** and well-maintained greenery, suggesting a well-developed and possibly a business or residential district.

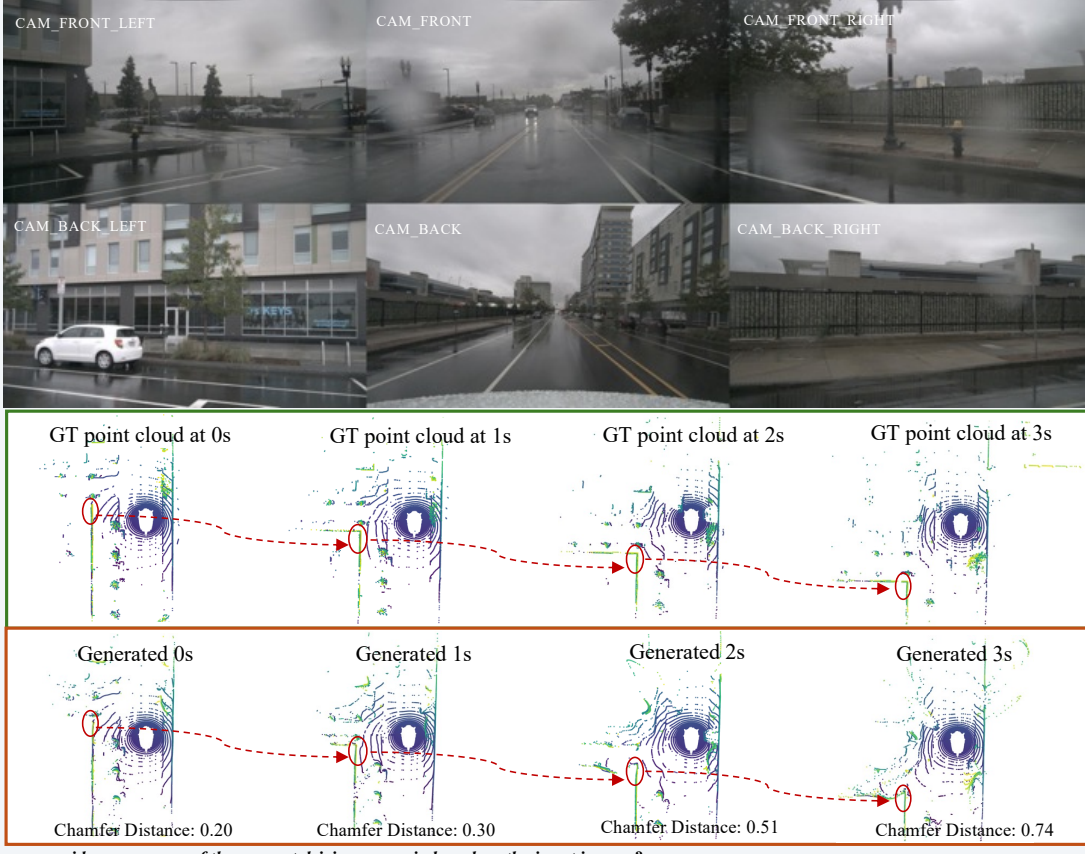
Q: Considering the clear road ahead and the traffic conditions, what would be the best driving practice in this scenario?

A: The best driving practice would be to continue at a moderate speed, maintain a safe following distance from the vehicle ahead, and stay vigilant for any potential movements from the **construction vehicle on the left**.

Q: What action should be taken in the current driving scenario?

A: In this situation, the vehicle should continue at a moderate speed and maintain the current lane.
 - Proceed straight, following the road markings and keeping a safe distance from the vehicles ahead.
 - Be aware of potential movements from the construction vehicle on the left, in case it starts to move or workers step onto the road.
 - Regularly check the rearview mirror to stay informed about the traffic situation behind, even though there's no immediate pressure from following vehicles.
 - Since the road ahead is clear, **focus on any unexpected obstacles that may appear from the sides of the road or from the construction area**.

(a)



Q: Can you provide a summary of the current driving scenario based on the input images?

A: The vehicle is positioned on a **multi-lane road** with clear lane markings, driving straight ahead against a backdrop of urban buildings under an overcast sky, suggesting it might be a cloudy day or early evening. The **road appears wet**, indicating recent rain, which could affect driving conditions. To the left, a **parking lot with several cars** is visible, while on the right, a **pedestrian sidewalk** is bordered by a **fence**, beyond which lies a large building complex. The road ahead is relatively clear, with a few vehicles in the distance and no immediate obstructions. In the rear view, the road is also clear with no vehicles in close proximity, and the surroundings are consistent with the front view, **featuring urban infrastructure and wet road conditions**.

Q: What kind of buildings are visible on the left side of the road?

A: On the left side of the road, there are **multi-story urban buildings** that appear to be commercial or residential.

Q: Is there any on-street parking visible?

A: Yes, there is a **parking lot visible to the left of the vehicle**, with several cars parked.

Q: Are there any visible traffic signs or signals?

A: **No traffic signs or signals** are visible from the current perspective.

Q: Can you see any pedestrians in the vicinity?

A: **No pedestrians** are visible in the immediate vicinity of the vehicle.

Q: How would you describe the weather conditions?

A: The weather is overcast, and the **road is wet, suggesting recent rainfall**.

Q: Is there any visible movement behind the vehicle?

A: No, there is **no visible movement behind** the vehicle; the road appears clear.

Q: What type of road markings can you see on the road ahead?

A: There are **white lane** markings on the road ahead, indicating the separation of lanes and the direction of traffic flow.

Q: Considering the wet road conditions, what driving behavior should be adopted?

A: The driver should maintain a moderate speed, increase following distance, and stay vigilant for pedestrians and other potential hazards due to the reduced traction on wet roads.

Q: Are there any indications of a residential area nearby?

A: Yes, the presence of a **large building complex to the left** suggests there may be a residential area nearby.

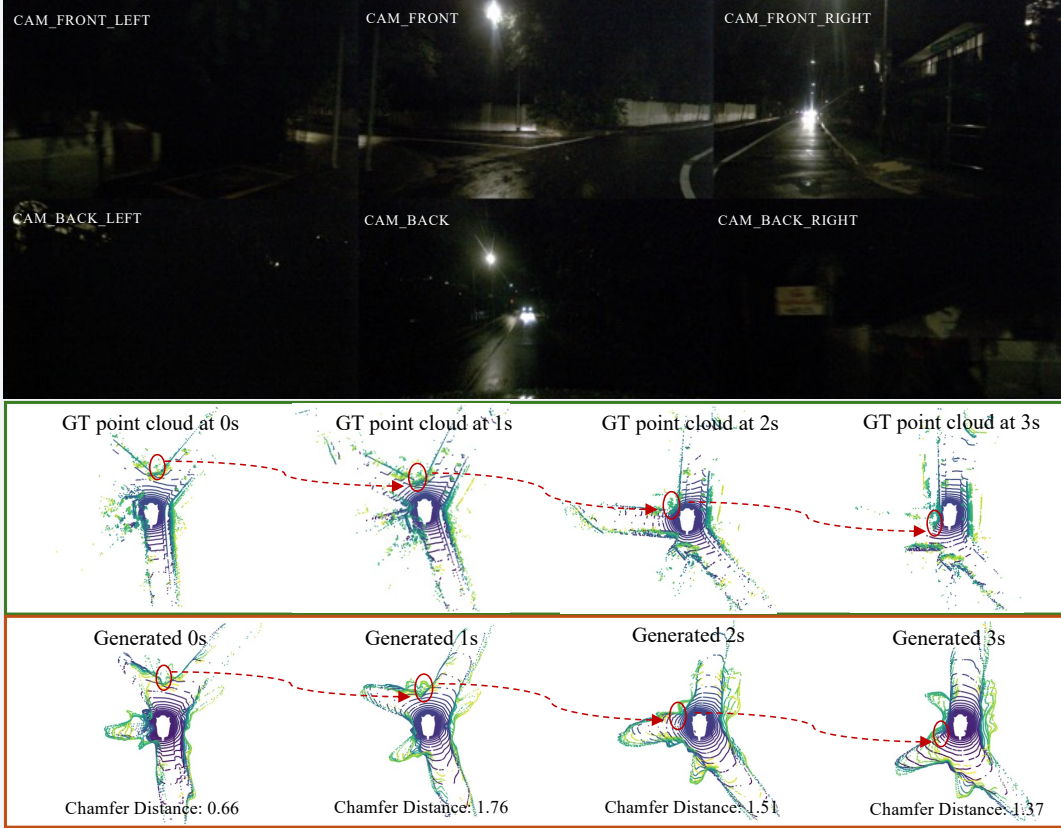
Q: What does the presence of a fence on the right-rear indicate?

A: The **fence on the right-rear** indicates a boundary for the public or private property adjacent to the road.

Q: What action should be taken in the current driving scenario?

A: Given the current road and weather conditions, the vehicle should:
- Maintain a moderate speed to account for the wet road surface, which could increase stopping distances.
- Stay in the current lane, following the clear lane markings to ensure a safe distance from other vehicles.
- Proceed straight, as there are no immediate turns or intersections visible.
- Remain vigilant for any pedestrians that may unexpectedly enter the roadway, especially given the reduced visibility from the weather conditions.

(b)



Q: Can you provide a summary of the current driving scenario based on the input images?

A: The environment is enveloped in the **darkness of night**, with only **streetlights** and the **headlights of vehicles** providing illumination. Directly ahead, the road is **glistening with moisture**, suggesting recent rain, and it appears to be slick, requiring careful navigation. To the right, the **glow of tail lights** indicates the presence of other vehicles, possibly moving or parked along the side of the road. On the left, the **road curves, hinting at a right turn ahead**. The rear views show **no immediate signs of traffic**, but the low visibility necessitates heightened awareness of any potential vehicles or obstacles that may be obscured by the darkness.

Q: Are there any traffic lights or stop signs visible?

A: **No traffic lights or stop signs are visible** in the immediate vicinity, indicating the absence of immediate traffic control devices in this section of the road.

Q: Can you describe any road signs and their possible meanings?

A: There are a few road signs visible, such as a 'No Entry' sign for a side road which suggests that it is not a through street and other regulatory signs that may not be fully visible due to the darkness.

Q: What is the condition of the road surface, and how should it affect driving behavior?

A: The **road surface is wet**, likely from recent rain, which should lead to a more cautious driving approach with reduced speed to prevent skidding.

Q: Is there any other vehicle around you?

A: Yes, there are **headlights visible in the distance** from another vehicle, suggesting there are cars on the road, but there are no vehicles in close proximity to us.

Q: Considering the wet road conditions and the solitary oncoming vehicle, what precautions should the driver take?

A: The driver should maintain a lower speed to account for **longer stopping distances on wet roads**, use headlights to increase visibility, and be vigilant for the oncoming vehicle, ready to react if it enters our lane.

Q: What can be inferred about the area surrounding the road?

A: The presence of trees and sparse buildings, along with the lack of immediate traffic in the rear views, suggests that this is a suburban or semi-rural area with lower traffic density.

Q: Is there any immediate traffic behind the vehicle?

A: There is no immediate traffic visible directly behind the vehicle, as the rear views show a clear path with **no other vehicles in close proximity**.

Q: How should the driver execute a right turn in these conditions?

A: The driver should signal well in advance, **reduce speed due to the wet road**, and check mirrors and blind spots for unseen traffic or cyclists before making the right turn.

Q: What action should be taken in the current driving scenario?

A: Given the low-light conditions and wet road, the vehicle should proceed with caution, preparing for a right turn.
 - Ensure the headlights and taillights are on for visibility.
 - Slow down to account for the longer stopping distance on the wet road surface.
 - Check the right side mirror and blind spot for any cyclists or vehicles that may be approaching from behind.
 - Signal well in advance to inform any possible vehicles behind of the intention to turn right.

(c)

Figure S2. Qualitative results for future generation and scene understanding. From top to bottom, each sub-figure displays the multi-view input of the current scene, the ground truth scene evolution, the generated scene evolution, and the scene understanding result.

References

- [1] Josh Achiam, Steven Adler, Sandhini Agarwal, Lama Ahmad, Ilge Akkaya, Florencia Leoni Aleman, Diogo Almeida, Janko Altenschmidt, Sam Altman, Shyamal Anadkat, et al. Gpt-4 technical report. *arXiv:2303.08774*, 2023. 3
- [2] Ben Agro, Quinlan Sykora, Sergio Casas, Thomas Gilles, and Raquel Urtasun. Uno: Unsupervised occupancy fields for perception and forecasting. In *Proc. of IEEE Intl. Conf. on Computer Vision and Pattern Recognition*, 2024. 3
- [3] Satanjeev Banerjee and Alon Lavie. Meteor: An automatic metric for mt evaluation with improved correlation with human judgments. In *Proc. Annual Meeting of the Association for Computational Linguistics Workshop*, 2005. 6
- [4] Holger Caesar, Varun Bankiti, Alex H Lang, Sourabh Vora, Venice Erin Liong, Qiang Xu, Anush Krishnan, Yu Pan, Giacomo Baldan, and Oscar Beijbom. nuscenes: A multi-modal dataset for autonomous driving. In *Proc. of IEEE Intl. Conf. on Computer Vision and Pattern Recognition*, 2020. 2, 5
- [5] Zhe Chen, Weiyun Wang, Hao Tian, Shenglong Ye, Zhangwei Gao, Erfei Cui, Wenwen Tong, Kongzhi Hu, Jiapeng Luo, Zheng Ma, et al. How far are we to gpt-4v? closing the gap to commercial multimodal models with open-source suites. *arXiv:2404.16821*, 2024. 5, 9
- [6] Zhe Chen, Jiannan Wu, Wenhui Wang, Weijie Su, Guo Chen, Sen Xing, Muyan Zhong, Qinglong Zhang, Xizhou Zhu, Lewei Lu, et al. Internvl: Scaling up vision foundation models and aligning for generic visual-linguistic tasks. In *Proc. of IEEE Intl. Conf. on Computer Vision and Pattern Recognition*, 2024. 2, 9
- [7] Mehdi Cherti, Romain Beaumont, Ross Wightman, Mitchell Wortsman, Gabriel Ilharco, Cade Gordon, Christoph Schuhmann, Ludwig Schmidt, and Jenia Jitsev. Reproducible scaling laws for contrastive language-image learning. In *Proc. of IEEE Intl. Conf. on Computer Vision and Pattern Recognition*, 2023. 3, 9
- [8] Xinpeng Ding, Jianhua Han, Hang Xu, Xiaodan Liang, Wei Zhang, and Xiaomeng Li. Holistic autonomous driving understanding by bird's-eye-view injected multi-modal large models. In *Proc. of IEEE Intl. Conf. on Computer Vision and Pattern Recognition*, 2024. 3
- [9] Runpei Dong, Chunrui Han, Yuang Peng, Zekun Qi, Zheng Ge, Jinrong Yang, Liang Zhao, Jianjian Sun, Hongyu Zhou, Haoran Wei, et al. Dreamllm: Synergistic multimodal comprehension and creation. In *Proc. of Intl. Conf. on Learning Representations*, 2024. 3
- [10] Yuxin Fang, Quan Sun, Xinggang Wang, Tiejun Huang, Xinglong Wang, and Yue Cao. Eva-02: A visual representation for neon genesis. *Image and Vision Computing*, 2024. 6
- [11] Ruiyuan Gao, Kai Chen, Enze Xie, Lanqing Hong, Zhenguo Li, Dit-Yan Yeung, and Qiang Xu. Magicdrive: Street view generation with diverse 3d geometry control. In *Proc. of Intl. Conf. on Learning Representations*, 2024. 2
- [12] Shenyuan Gao, Jiazhi Yang, Li Chen, Kashyap Chitta, Yihang Qiu, Andreas Geiger, Jun Zhang, and Hongyang Li. Vista: A generalizable driving world model with high fidelity and versatile controllability. In *Proc. of Advances in Neural Information Processing Systems*, 2024. 1, 2
- [13] Songen Gu, Wei Yin, Bu Jin, Xiaoyang Guo, Junming Wang, Haodong Li, Qian Zhang, and Xiaoxiao Long. Dome: Tampering diffusion model into high-fidelity controllable occupancy world model. *arXiv:2410.10429*, 2024. 3
- [14] David Ha and Jürgen Schmidhuber. World models. In *Proc. of Advances in Neural Information Processing Systems*, 2018. 2
- [15] Jinghua Hou, Zhe Liu, Zhikang Zou, Xiaoqing Ye, Xiang Bai, et al. Query-based temporal fusion with explicit motion for 3d object detection. *Proc. of Advances in Neural Information Processing Systems*, 36:75782–75797, 2023. 1
- [16] Anthony Hu, Lloyd Russell, Hudson Yeo, Zak Murez, George Fedoseev, Alex Kendall, Jamie Shotton, and Gianluca Corrado. Gaia-1: A generative world model for autonomous driving. *arXiv:2309.17080*, 2023. 1, 2
- [17] Edward J Hu, Phillip Wallis, Zeyuan Allen-Zhu, Yuanzhi Li, Shean Wang, Lu Wang, Weizhu Chen, et al. Lora: Low-rank adaptation of large language models. In *Proc. of Intl. Conf. on Learning Representations*, 2021. 9
- [18] Zhijian Huang, Chengjian Feng, Feng Yan, Baihui Xiao, Zequn Jie, Yujie Zhong, Xiaodan Liang, and Lin Ma. Drivemm: All-in-one large multimodal model for autonomous driving. *arXiv:2412.07689*, 2024. 6
- [19] Zanming Huang, Jimuyang Zhang, and Eshed Ohn-Bar. Neural volumetric world models for autonomous driving. In *Proc. of European Conference on Computer Vision*, 2024. 3
- [20] Aaron Hurst, Adam Lerer, Adam P Goucher, Adam Perelman, Aditya Ramesh, Aidan Clark, AJ Ostrow, Akila Welihinda, Alan Hayes, Alec Radford, et al. Gpt-4o system card. *arXiv:2410.21276*, 2024. 6
- [21] Fan Jia, Weixin Mao, Yingfei Liu, Yucheng Zhao, Yuqing Wen, Chi Zhang, Xiangyu Zhang, and Tiancai Wang. Adriver-i: A general world model for autonomous driving. *arXiv:2311.13549*, 2023. 2
- [22] Tarasha Khurana, Peiyun Hu, David Held, and Deva Ramanan. Point cloud forecasting as a proxy for 4d occupancy forecasting. In *Proc. of IEEE Intl. Conf. on Computer Vision and Pattern Recognition*, 2023. 1, 3, 6
- [23] Bo Li, Yuanhan Zhang, Dong Guo, Renrui Zhang, Feng Li, Hao Zhang, Kaichen Zhang, Peiyuan Zhang, Yanwei Li, Ziwei Liu, et al. Llava-onevision: Easy visual task transfer. *arXiv:2408.03326*, 2024. 6
- [24] Jingyu Li, Zhe Liu, Jinghua Hou, and Dingkang Liang. Dds3d: Dense pseudo-labels with dynamic threshold for semi-supervised 3d object detection. In *Proc. of the IEEE Int. Conf. on Robotics and Automation*, pages 9245–9252, 2023. 1
- [25] Xiaofan Li, Yifu Zhang, and Xiaoqing Ye. Drivingdiffusion: Layout-guided multi-view driving scenarios video generation with latent diffusion model. In *Proc. of European Conference on Computer Vision*, 2024. 2
- [26] Zhiqi Li, Wenhui Wang, Hongyang Li, Enze Xie, Chonghao Sima, Tong Lu, Yu Qiao, and Jifeng Dai. Bevformer: Learning bird's-eye-view representation from multi-camera images via spatiotemporal transformers. In *Proc. of European Conference on Computer Vision*, 2022. 3

- [27] Zhang Li, Biao Yang, Qiang Liu, Zhiyin Ma, Shuo Zhang, Jingxu Yang, Yabo Sun, Yuliang Liu, and Xiang Bai. Monkey: Image resolution and text label are important things for large multi-modal models. In *Proc. of IEEE Intl. Conf. on Computer Vision and Pattern Recognition*, 2024. 2, 5
- [28] Dingkang Liang, Tianrui Feng, Xin Zhou, Yumeng Zhang, Zhikang Zou, and Xiang Bai. Parameter-efficient fine-tuning in spectral domain for point cloud learning. *IEEE Transactions on Pattern Analysis and Machine Intelligence*, 2025. 1
- [29] Chin-Yew Lin. Rouge: A package for automatic evaluation of summaries. In *Proc. Annual Meeting of the Association for Computational Linguistics Workshop*, 2004. 6
- [30] Haotian Liu, Chunyuan Li, Qingyang Wu, and Yong Jae Lee. Visual instruction tuning. In *Proc. of Advances in Neural Information Processing Systems*, pages 34892–34916, 2023. 10
- [31] Haotian Liu, Chunyuan Li, Qingyang Wu, and Yong Jae Lee. Visual instruction tuning. In *Proc. of Advances in Neural Information Processing Systems*, 2023. 2, 5
- [32] Haotian Liu, Chunyuan Li, Yuheng Li, and Yong Jae Lee. Improved baselines with visual instruction tuning. In *Proc. of IEEE Intl. Conf. on Computer Vision and Pattern Recognition*, pages 26296–26306, 2024. 5
- [33] Zhuang Liu, Hanzi Mao, Chao-Yuan Wu, Christoph Feichtenhofer, Trevor Darrell, and Saining Xie. A convnet for the 2020s. In *Proc. of IEEE Intl. Conf. on Computer Vision and Pattern Recognition*, 2022. 3, 9
- [34] Jiachen Lu, Ze Huang, Zeyu Yang, Jiahui Zhang, and Li Zhang. Wovogen: World volume-aware diffusion for controllable multi-camera driving scene generation. In *Proc. of European Conference on Computer Vision*, 2024. 2
- [35] Enhui Ma, Lijun Zhou, Tao Tang, Zhan Zhang, Dong Han, Junpeng Jiang, Kun Zhan, Peng Jia, Xianpeng Lang, Haiyang Sun, et al. Unleashing generalization of end-to-end autonomous driving with controllable long video generation. *arXiv:2406.01349*, 2024. 2
- [36] Junyi Ma, Xieyuanli Chen, Jiawei Huang, Jingyi Xu, Zhen Luo, Jintao Xu, Weihao Gu, Rui Ai, and Hesheng Wang. Cam4docc: Benchmark for camera-only 4d occupancy forecasting in autonomous driving applications. In *Proc. of IEEE Intl. Conf. on Computer Vision and Pattern Recognition*, 2024. 2
- [37] Chen Min, Dawei Zhao, Liang Xiao, Jian Zhao, Xinli Xu, Zheng Zhu, Lei Jin, Jianshu Li, Yulan Guo, Junliang Xing, et al. Driveworld: 4d pre-trained scene understanding via world models for autonomous driving. In *Proc. of IEEE Intl. Conf. on Computer Vision and Pattern Recognition*, 2024. 2
- [38] Ming Nie, Renyuan Peng, Chunwei Wang, Xinyue Cai, Jianhua Han, Hang Xu, and Li Zhang. Reason2drive: Towards interpretable and chain-based reasoning for autonomous driving. In *Proc. of European Conference on Computer Vision*, 2024. 3
- [39] Jinhyung Park, Chenfeng Xu, Shijia Yang, Kurt Keutzer, Kris Kitani, Masayoshi Tomizuka, and Wei Zhan. Time will tell: New outlooks and a baseline for temporal multi-view 3d object detection. In *Proc. of Intl. Conf. on Learning Representations*, 2022. 6
- [40] Jonah Philion and Sanja Fidler. Lift, splat, shoot: Encoding images from arbitrary camera rigs by implicitly unprojecting to 3d. In *Proc. of European Conference on Computer Vision*, 2020. 6
- [41] Tianwen Qian, Jingjing Chen, Linhai Zhuo, Yang Jiao, and Yu-Gang Jiang. Nuscenes-qa: A multi-modal visual question answering benchmark for autonomous driving scenario. In *Proc. of the AAAI Conf. on Artificial Intelligence*, pages 4542–4550, 2024. 10
- [42] Alec Radford, Jong Wook Kim, Chris Hallacy, Aditya Ramesh, Gabriel Goh, Sandhini Agarwal, Girish Sastry, Amanda Askell, Pamela Mishkin, Jack Clark, et al. Learning transferable visual models from natural language supervision. In *Proc. of Intl. Conf. on Machine Learning*, 2021. 7, 9
- [43] Hao Shao, Yuxuan Hu, Letian Wang, Guanglu Song, Steven L Waslander, Yu Liu, and Hongsheng Li. Lmdrive: Closed-loop end-to-end driving with large language models. In *Proc. of IEEE Intl. Conf. on Computer Vision and Pattern Recognition*, 2024. 3
- [44] Chonghao Sima, Katrin Renz, Kashyap Chitta, Li Chen, Hanxue Zhang, Chengan Xie, Jens Beißenwenger, Ping Luo, Andreas Geiger, and Hongyang Li. Drivelm: Driving with graph visual question answering. In *Proc. of European Conference on Computer Vision*, 2024. 2, 3
- [45] Ashish Vaswani, Noam Shazeer, Niki Parmar, Jakob Uszkoreit, Llion Jones, Aidan N Gomez, Łukasz Kaiser, and Illia Polosukhin. Attention is all you need. In *Proc. of Advances in Neural Information Processing Systems*, 2017. 7
- [46] Ramakrishna Vedantam, C Lawrence Zitnick, and Devi Parikh. Cider: Consensus-based image description evaluation. In *Proc. of IEEE Intl. Conf. on Computer Vision and Pattern Recognition*, 2015. 6
- [47] Lening Wang, Wenzhao Zheng, Yilong Ren, Han Jiang, Zhiyong Cui, Haiyang Yu, and Jiwen Lu. Occsora: 4d occupancy generation models as world simulators for autonomous driving. *arXiv:2405.20337*, 2024. 3
- [48] Peng Wang, Lingjie Liu, Yuan Liu, Christian Theobalt, Taku Komura, and Wenping Wang. Neus: Learning neural implicit surfaces by volume rendering for multi-view reconstruction. In *Proc. of Advances in Neural Information Processing Systems*, 2021. 3, 4
- [49] Shihao Wang, Yingfei Liu, Tiancai Wang, Ying Li, and Xiangyu Zhang. Exploring object-centric temporal modeling for efficient multi-view 3d object detection. In *Proc. of IEEE Intl. Conf. on Computer Vision*, 2023. 6
- [50] Shihao Wang, Zhiding Yu, Xiaohui Jiang, Shiyi Lan, Min Shi, Nadine Chang, Jan Kautz, Ying Li, and Jose M Alvarez. Omnidrive: A holistic llm-agent framework for autonomous driving with 3d perception, reasoning and planning. In *Proc. of IEEE Intl. Conf. on Computer Vision and Pattern Recognition*, 2025. 2, 3, 5, 6, 9, 10
- [51] Tai Wang, Xinge Zhu, Jiangmiao Pang, and Dahua Lin. Fcos3d: Fully convolutional one-stage monocular 3d object detection. In *Proc. of IEEE Intl. Conf. on Computer Vision*, 2021. 6
- [52] Wenhui Wang, Jiangwei Xie, ChuanYang Hu, Haoming Zou, Jianan Fan, Wenwen Tong, Yang Wen, Silei Wu, Hanming

- Deng, Zhiqi Li, et al. Drivemlm: Aligning multi-modal large language models with behavioral planning states for autonomous driving. *arXiv:2312.09245*, 2023. 3
- [53] Xiaofeng Wang, Zheng Zhu, Guan Huang, Xinze Chen, Jia-gang Zhu, and Jiwen Lu. Drivedreamer: Towards real-world-driven world models for autonomous driving. In *Proc. of European Conference on Computer Vision*, 2024. 2
- [54] Yuqi Wang, Jiawei He, Lue Fan, Hongxin Li, Yuntao Chen, and Zhaoxiang Zhang. Driving into the future: Multiview visual forecasting and planning with world model for autonomous driving. In *Proc. of IEEE Intl. Conf. on Computer Vision and Pattern Recognition*, 2024. 1, 2
- [55] Julong Wei, Shanshuai Yuan, Pengfei Li, Qingda Hu, Zhongxue Gan, and Wenchoao Ding. Occllama: An occupancy-language-action generative world model for autonomous driving. *arXiv:2409.03272*, 2024. 3
- [56] Yuqing Wen, Yucheng Zhao, Yingfei Liu, Fan Jia, Yan-hui Wang, Chong Luo, Chi Zhang, Tiancai Wang, Xiaoyan Sun, and Xiangyu Zhang. Panacea: Panoramic and controllable video generation for autonomous driving. In *Proc. of IEEE Intl. Conf. on Computer Vision and Pattern Recognition*, 2024. 2
- [57] Xinshuo Weng, Junyu Nan, Kuan-Hui Lee, Rowan McAllister, Adrien Gaidon, Nicholas Rhinehart, and Kris M Kitani. S2net: Stochastic sequential pointcloud forecasting. In *Proc. of European Conference on Computer Vision*, 2022. 1, 3
- [58] Jiannan Wu, Muyan Zhong, Sen Xing, Zeqiang Lai, Zhaoyang Liu, Wenhui Wang, Zhe Chen, Xizhou Zhu, Lewei Lu, Tong Lu, et al. Visionllm v2: An end-to-end generalist multimodal large language model for hundreds of vision-language tasks. In *Proc. of Advances in Neural Information Processing Systems*, 2024. 3
- [59] Zhenhua Xu, Yujia Zhang, Enze Xie, Zhen Zhao, Yong Guo, Kwan-Yee K Wong, Zhenguo Li, and Hengshuang Zhao. Drivegpt4: Interpretable end-to-end autonomous driving via large language model. *IEEE Robotics and Automation Letters*, 2024. 3
- [60] Ziyang Yan, Wenzhen Dong, Yihua Shao, Yuhang Lu, Liu Haiyang, Jingwen Liu, Haozhe Wang, Zhe Wang, Yan Wang, Fabio Remondino, et al. Renderworld: World model with self-supervised 3d label. *arXiv:2409.11356*, 2024. 3
- [61] Chenyu Yang, Yuntao Chen, Hao Tian, Chenxin Tao, Xizhou Zhu, Zhaoxiang Zhang, Gao Huang, Hongyang Li, Yu Qiao, Lewei Lu, et al. Bevformer v2: Adapting modern image backbones to bird's-eye-view recognition via perspective supervision. In *Proc. of IEEE Intl. Conf. on Computer Vision and Pattern Recognition*, 2023. 3, 9
- [62] Honghui Yang, Sha Zhang, Di Huang, Xiaoyang Wu, Haoyi Zhu, Tong He, Shixiang Tang, Hengshuang Zhao, Qibo Qiu, Binbin Lin, et al. Unipad: A universal pre-training paradigm for autonomous driving. In *Proc. of IEEE Intl. Conf. on Computer Vision and Pattern Recognition*, 2024. 3, 4
- [63] Jiazh Yang, Shenyuan Gao, Yihang Qiu, Li Chen, Tianyu Li, Bo Dai, Kashyap Chitta, Penghao Wu, Jia Zeng, Ping Luo, et al. Generalized predictive model for autonomous driving. In *Proc. of IEEE Intl. Conf. on Computer Vision and Pattern Recognition*, 2024. 2
- [64] Senqiao Yang, Jiaming Liu, Ray Zhang, Mingjie Pan, Zoey Guo, Xiaoqi Li, Zehui Chen, Peng Gao, Yandong Guo, and Shanghang Zhang. Lidar-llm: Exploring the potential of large language models for 3d lidar understanding. *arXiv preprint arXiv:2312.14074*, 2023. 10
- [65] Zetong Yang, Li Chen, Yanan Sun, and Hongyang Li. Visual point cloud forecasting enables scalable autonomous driving. In *Proc. of IEEE Intl. Conf. on Computer Vision and Pattern Recognition*, 2024. 1, 2, 3, 6, 10
- [66] Dingyuan Zhang, Dingkang Liang, Zichang Tan, Xiaoqing Ye, Cheng Zhang, Jingdong Wang, and Xiang Bai. Make your vit-based multi-view 3d detectors faster via token compression. In *Proc. of European Conference on Computer Vision*, pages 56–72, 2024. 4
- [67] Lunjun Zhang, Yuwen Xiong, Ze Yang, Sergio Casas, Rui Hu, and Raquel Urtasun. Learning unsupervised world models for autonomous driving via discrete diffusion. In *Proc. of Intl. Conf. on Learning Representations*, 2023. 1, 3
- [68] Yumeng Zhang, Shi Gong, Kaixin Xiong, Xiaoqing Ye, Xiao Tan, Fan Wang, Jizhou Huang, Hua Wu, and Haifeng Wang. Bevworld: A multimodal world model for autonomous driving via unified bev latent space. *arXiv:2407.05679*, 2024. 2
- [69] Zheng Zhang, Yeyao Ma, Enming Zhang, and Xiang Bai. Psalm: Pixelwise segmentation with large multi-modal model. In *Proc. of European Conference on Computer Vision*, 2024. 3
- [70] Guosheng Zhao, Xiaofeng Wang, Zheng Zhu, Xinze Chen, Guan Huang, Xiaoyi Bao, and Xingang Wang. Drivedreamer-2: Llm-enhanced world models for diverse driving video generation. *arXiv:2403.06845*, 2024. 1, 2
- [71] Zongchuang Zhao, Haoyu Fu, Dingkang Liang, Xin Zhou, Dingyuan Zhang, Hongwei Xie, Bing Wang, and Xiang Bai. Extending large vision-language model for diverse interactive tasks in autonomous driving. *arXiv:2505.08725*, 2025. 5, 9
- [72] Wenzhao Zheng, Weiliang Chen, Yuanhui Huang, Borui Zhang, Yueqi Duan, and Jiwen Lu. Occworld: Learning a 3d occupancy world model for autonomous driving. In *Proc. of European Conference on Computer Vision*, 2024. 3
- [73] Wenzhao Zheng, Zetian Xia, Yuanhui Huang, Sicheng Zuo, Jie Zhou, and Jiwen Lu. Doe-1: Closed-loop autonomous driving with large world model. *arXiv:2412.09627*, 2024. 2
- [74] Yunsong Zhou, Linyan Huang, Qingwen Bu, Jia Zeng, Tianyu Li, Hang Qiu, Hongzi Zhu, Minyi Guo, Yu Qiao, and Hongyang Li. Embodied understanding of driving scenarios. In *Proc. of European Conference on Computer Vision*, pages 129–148, 2024. 3
- [75] Haoyi Zhu, Honghui Yang, Xiaoyang Wu, Di Huang, Sha Zhang, Xianglong He, Tong He, Hengshuang Zhao, Chunhua Shen, Yu Qiao, et al. Ponderv2: Pave the way for 3d foundation model with a universal pre-training paradigm. *arXiv:2310.08586*, 2023. 3, 4
- [76] Vlas Zyrianov, Henry Che, Zhijian Liu, and Shenlong Wang. Lidardm: Generative lidar simulation in a generated world. *arXiv:2404.02903*, 2024. 1, 3